Signal Processing 93 (2013) 641–651

Contents lists available at SciVerse ScienceDirect

Signal Processing

journal homepage: www.elsevier.com/locate/sigpro

Beamspace direction finding based on the conjugate gradient and the auxiliary vector filtering algorithms ☆, ☆☆

Jens Steinwandt [a,*], Rodrigo C. de Lamare [b], Martin Haardt [a]

[a] Communications Research Laboratory, Ilmenau University of Technology, P.O. Box 100565, 98684 Ilmenau, Germany
[b] Communications Research Group, Department of Electronics, University of York, York YO10 5DD, United Kingdom

ARTICLE INFO

Article history:
Received 2 February 2012
Received in revised form
30 July 2012
Accepted 2 September 2012
Available online 10 September 2012

Keywords:
Direction of arrival estimation
Beamspace processing
Krylov subspace
Conjugate gradient
Auxiliary vector filtering

ABSTRACT

Motivated by the performance of the direction finding algorithms based on the auxiliary vector filtering (AVF) method and the conjugate gradient (CG) method as well as the advantages of operating in beamspace (BS), we develop two novel direction finding algorithms for uniform linear arrays (ULAs) in the beamspace domain, which we refer to as the BS AVF and the BS CG methods. The recently proposed Krylov subspace-based CG and AVF algorithms for the direction of arrival (DOA) estimation utilize a non-eigenvector basis to generate the signal subspace and yield a superior resolution performance for closely spaced sources under severe conditions. However, their computational complexity is similar to the eigenvector-based methods. In order to save computational resources, we perform a dimension reduction through the linear transformation into the beamspace domain, which additionally leads to significant improvements in terms of the resolution capability and the estimation accuracy. A comprehensive complexity analysis and simulation results demonstrate the excellent performance of the proposed algorithms and show their computational requirements. As examples, we investigate the efficacy of the developed methods for the discrete Fourier transform (DFT) and the discrete prolate spheroidal sequences (DPSS) beamspace designs.

1. Introduction

The need for the direction of arrival (DOA) estimation of incident signal wavefronts using sensor arrays is encountered in a broad range of important applications, including radar, wireless communications, biomedicine, etc. As a result, numerous methods for estimating the DOAs of signals have been proposed in the last few decades [1]. Among the most powerful techniques are the subspace-based algorithms, such as MUSIC [2], Root-MUSIC [3] and ESPRIT [4], which are proven to yield high-resolution capabilities. However, they require an eigendecomposition of the $M \times M$ spatial covariance matrix $\boldsymbol{R} = \mathbb{E}\{\boldsymbol{x}\boldsymbol{x}^H\}$ of the received data, corresponding to M sensor elements. As this is a computationally expensive operation with $\mathcal{O}(M^3 + M^2 N)$ multiplications, a new class of subspace-based DOA estimation methods termed Krylov subspace-based methods [5,6], adopting the auxiliary vector filtering (AVF) algorithm [7] or, as an extension, the conjugate gradient (CG) algorithm [8], was recently proposed. Note that another class of DOA

☆ Parts of this paper have been published at the IEEE International ITG Workshop on Smart Antennas (WSA 2011), Aachen, Germany, February 2011.

☆☆ This work was supported by the International Graduate School on Mobile Communications (MOBICOM), Ilmenau, Germany.

* Corresponding author. Tel.: +49 3677 69 2613; fax: +49 3677 69 1195.
E-mail addresses: Jens.Steinwandt@tu-ilmenau.de (J. Steinwandt), rcdl500@ohm.york.ac.uk (R.C. de Lamare), martin.haardt@tu-ilmenau.de (M. Haardt).
URL: http://www.tu-ilmenau.de/crl (J. Steinwandt).

0165-1684/$ - see front matter © 2012 Elsevier B.V. All rights reserved.
http://dx.doi.org/10.1016/j.sigpro.2012.09.001

estimators that do not resort to an eigendecomposition but still demand a high computational cost comprises the maximum-likelihood (ML) methods [1,9,10]. Here, however, we only focus on the subspace-based algorithms.

The advantage of the Krylov-based techniques is that they are applicable to arbitrary array geometries and avoid the eigendecomposition by iteratively generating an extended Krylov signal subspace that consists of the true signal subspace and the scanning vector itself. While the AVF algorithm forms the signal subspace from auxiliary vectors, the CG method applies residual vectors to span the Krylov subspace. Then, the unknown DOAs are determined by the search for the rank collapse of the extended signal subspace in the entire spatial spectrum, which occurs when the scanning vector is contained in it. This results in superior resolution performance for closely spaced sources under severe conditions, i.e., in the case of a low signal-to-noise ratio (SNR) and a small data record. However, despite utilizing a non-eigenvector basis they suffer from a similar computational complexity as the eigenvector-based methods, since the Krylov signal subspace is constructed for each search angle.

One way of significantly reducing the computational complexity is beamspace (BS) processing [11], which transforms the original data in element space into a reduced-dimensional subspace and performs the DOA estimation only in a spatial sector rather than in the entire angle range. Apart from the great computational savings, operation in beamspace also increases the resolution abilities as well as the estimation accuracy [12]. This is achieved by the enhancement of the SNR within the spatial sector of interest in analogy to beamforming. However, it is well known that beamspace processing does not improve the best achievable estimation accuracy as it only preserves the signals in the sector of interest, i.e., the corresponding Cramér–Rao lower bound (CRLB) in beamspace is equal to the element-space CRLB if there are only in-sector sources [13,14]. Beamspace techniques with robustness against strong sources that are located outside of the spatial sector were developed in [15,16].

In this paper, we propose two beamspace direction finding algorithms based on the CG and the AVF algorithms. Note that although these two Krylov-based algorithms are applicable to arbitrary array geometries we focus on uniform linear arrays (ULA) in this work to simplify the operation in beamspace. A generalization to other geometries can be achieved by considering array linearization techniques [17] prior to the proposed beamspace algorithms. Also, our methods are designed for the one-dimensional DOA estimation but extensions to the two-dimensional case are possible. For convenience, we assume that the number of signal sources d is known and that they are well inside the subband of interest. As the search for the signals is only conducted in a spatial sector, either a priori information of the approximate position of the DOAs is required or parallel processing of overlapping sectors of the angle spectrum has to be applied. We show that the proposed algorithms require a substantially lower computational complexity compared to their counterparts in element space. Moreover, they provide a better resolution and better estimation capabilities compared to previously developed beamspace algorithms, such as BS MUSIC [12], BS Root-MUSIC [18], and BS ESPRIT [19]. In addition, two different designs of the beamspace transformation matrix using the discrete Fourier transform (DFT) and discrete prolate spheroidal sequences (DPSS) are evaluated and compared.

The remainder of this paper is organized as follows. Section 2 describes the system model. The two different ways of designing the beamspace matrix are introduced and compared in Section 3. In Section 4, the proposed BS CG and BS AVF algorithms are presented, whereas Section 5 deals with the complexity analysis. Section 6 illustrates and discusses the simulation results and finally, the concluding remarks are drawn in Section 7.

Notation: We use lowercase boldface letters for column vectors and uppercase boldface letters for matrices. The superscripts T,* and H denote transpose, complex conjugate, and conjugate transpose, respectively, $\|\boldsymbol{x}\|$ represents the 2-norm of the vector $\boldsymbol{x}$ and $\mathbb{E}\{\cdot\}$ stands for the statistical expectation.

2. System model and beamspace processing

Let an M-element ULA receive narrowband signals originating from d ($d<M$) far-field sources with the DOAs $\boldsymbol{\theta}=[\theta_1,\ldots,\theta_d]^T$. The ith of N available data snapshots of the $M\times 1$ array output vector can be modeled as

$$\boldsymbol{x}(i)=\boldsymbol{A}(\boldsymbol{\theta})\boldsymbol{s}(i)+\boldsymbol{n}(i),\quad i=1,\ldots,N, \tag{1}$$

where $\boldsymbol{A}(\boldsymbol{\theta})=[\boldsymbol{a}(\theta_1),\ldots,\boldsymbol{a}(\theta_d)]\in\mathbb{C}^{M\times d}$ is the array steering matrix, $\boldsymbol{s}(i)=[s_1(i),\ldots,s_d(i)]^T\in\mathbb{C}^{d\times 1}$ represents the zero-mean vector of signal waveforms, and $\boldsymbol{n}(i)\in\mathbb{C}^{M\times 1}$ is the vector of white circularly symmetric complex Gaussian sensor noise with zero mean and variance σ_n^2. The $M\times 1$ steering vector $\boldsymbol{a}(\theta_l)$ corresponding to the lth source, $l=1,\ldots,d$, is expressed as

$$\boldsymbol{a}(\theta_l)=\left[1\;\; e^{\mathrm{j}2\pi(\Delta/\lambda_c)\sin\theta_l}\;\;\cdots\;\; e^{\mathrm{j}2\pi(M-1)(\Delta/\lambda_c)\sin\theta_l}\right]^T, \tag{2}$$

where Δ denotes the interelement spacing of the ULA, λ_c is the signal wavelength, and omni-directional sensors have been assumed for the sake of notational simplicity. Using the fact that $\boldsymbol{s}(i)$ and $\boldsymbol{n}(i)$ are modeled as uncorrelated random variables, the $M\times M$ covariance matrix is calculated by

$$\boldsymbol{R}=\mathbb{E}\{\boldsymbol{x}(i)\boldsymbol{x}^H(i)\}=\boldsymbol{A}(\boldsymbol{\theta})\boldsymbol{R}_{ss}\boldsymbol{A}^H(\boldsymbol{\theta})+\sigma_n^2\boldsymbol{I}_M, \tag{3}$$

where $\boldsymbol{R}_{ss}=\mathbb{E}\{\boldsymbol{s}(i)\boldsymbol{s}^H(i)\}$ and $\boldsymbol{I}_M$ is the $M\times M$ identity matrix. In practice, the unknown covariance matrix is estimated by the sample covariance matrix

$$\hat{\boldsymbol{R}}=\frac{1}{N}\sum_{i=1}^{N}\boldsymbol{x}(i)\boldsymbol{x}^H(i). \tag{4}$$

The linear transformation of the original data into the beamspace of a lower dimension B with $d<B<M$ is defined as

$$\tilde{\boldsymbol{x}}(i)=\boldsymbol{W}^H\boldsymbol{x}(i)\in\mathbb{C}^{B\times 1}, \tag{5}$$

where $\boldsymbol{W}$ is the $M\times B$ beamspace matrix satisfying $\boldsymbol{W}^H\boldsymbol{W}=\boldsymbol{I}_B$, so that the beamspace sensor noise remains spatially white. If the beamspace matrix $\boldsymbol{W}_o$ is not

unitary, additional noise prewhitening is required and a unitary $\boldsymbol{W}$ can be constructed as $\boldsymbol{W}=(\boldsymbol{W}_o^H\boldsymbol{W}_o)^{-1/2}\boldsymbol{W}_o^H$.

The $B\times B$ beamspace covariance matrix is given by

$$\tilde{\boldsymbol{R}}=\mathbb{E}\{\tilde{\boldsymbol{x}}(i)\tilde{\boldsymbol{x}}^H(i)\}=\boldsymbol{W}^H\boldsymbol{A}(\boldsymbol{\theta})\boldsymbol{R}_{ss}\boldsymbol{A}^H(\boldsymbol{\theta})\boldsymbol{W}+\sigma_n^2\boldsymbol{I}_B. \tag{6}$$

From (5) and (6), it is apparent that the beamspace transformation changes the original array manifold to

$$\tilde{\boldsymbol{a}}(\theta)=\boldsymbol{W}^H\boldsymbol{a}(\theta), \tag{7}$$

where $\tilde{\boldsymbol{a}}(\theta)$ is the new steering vector in the beamspace. The eigendecomposition of the sample estimate of (6) enables us to express $\tilde{\boldsymbol{R}}$ in terms of its eigenvectors and eigenvalues, i.e.,

$$\tilde{\boldsymbol{R}}=\tilde{\boldsymbol{U}}_s\tilde{\boldsymbol{\Lambda}}_s\tilde{\boldsymbol{U}}_s^H+\tilde{\boldsymbol{U}}_n\tilde{\boldsymbol{\Lambda}}_n\tilde{\boldsymbol{U}}_n^H, \tag{8}$$

where the diagonal matrices $\tilde{\boldsymbol{\Lambda}}_s$ and $\tilde{\boldsymbol{\Lambda}}_n$ contain the d largest eigenvalues and the $B-d$ smallest eigenvalues, respectively, and $\tilde{\boldsymbol{U}}_s$ and $\tilde{\boldsymbol{U}}_n$ contain their corresponding eigenvectors.

3. Beamspace design

In order to improve the resolution compared to the element space, the beamspace transformation matrix needs to be chosen adequately. The design of this matrix is determined by the beam pattern, which is constructed to suit different characteristics. More specifically, the columns of the transformation matrix $\boldsymbol{W}$ can be physically interpreted as beams pointing to different angles. Thus, the performance of the operation in beamspace depends on the properties of the beams. In this section, we review the DFT beamspace matrix, the DPSS transformation matrix, and compare them to each other.

3.1. DFT-based beamspace design

The most common preprocessing scheme is the $M\times B$ DFT matrix beamformer composed of B consecutive columns of the M-point DFT matrix. The output in the DFT beamspace is formed as

$$\tilde{\boldsymbol{x}}_{\mathrm{DFT}}(i)=\boldsymbol{W}_{\mathrm{DFT}_{B,m}}^H\boldsymbol{x}(i)\in\mathbb{C}^{B\times 1}, \tag{9}$$

where m denotes the first column of the DFT manifold $0\le m\le(M-1)$, and selects the sector of interest based on the prior knowledge. The subscripts B and m in $\boldsymbol{W}_{\mathrm{DFT}_{B,m}}$ are intended to clarify the dependence on the number of beams B and the subband m under consideration. The resulting orthogonal beam pointing angles are equispaced by the angular distance $\Delta u=2/M$, so that the DFT transformation matrix is given by

$$\boldsymbol{W}_{\mathrm{DFT}_{B,m}}=\left[\boldsymbol{w}\left(m\frac{2}{M}\right)\ \cdots\ \boldsymbol{w}\left((m+B-1)\frac{2}{M}\right)\right], \tag{10}$$

where the DFT beamforming vector $\boldsymbol{w}(u)$ exhibits the Vandermonde structure

$$\boldsymbol{w}(u)=\left[1\ \ e^{\mathrm{j}\pi u}\ \ \cdots\ \ e^{\mathrm{j}(M-1)\pi u}\right]^T\in\mathbb{C}^{M\times 1}, \tag{11}$$

with $u\in\{m(2/M),(m+1)(2/M),\ldots,(m+B-1)(2/M)\}$ defining the range of the spatial sector.

3.2. DPSS-based beamspace design

Discrete prolate spheroidal sequences were first applied to beamspace processing in [20]. The basic idea is to maximize the ratio of the energy within the desired sector defined by Θ to the total beamspace energy in the entire spatial domain described by $[-\pi,\pi]$, which can be formulated according to [14] as

$$\alpha_b\triangleq\frac{\int_\Theta|\boldsymbol{w}_b^H\boldsymbol{a}(\theta)|^2\,d\theta}{\int_{-\pi}^{\pi}|\boldsymbol{w}_b^H\boldsymbol{a}(\theta)|^2\,d\theta},\quad b=1,\ldots,B, \tag{12}$$

where $\boldsymbol{w}_b$ is the bth column of the DPSS transformation matrix $\boldsymbol{W}_{\mathrm{DPSS}_{B,\Theta}}$. Again, the subscripts highlight the dependence on B and the sector of interest Θ. Using the fact that for ULAs

$$\int_{-\pi}^{\pi}|\boldsymbol{w}_b^H\boldsymbol{a}(\theta)|^2\,d\theta=2\pi\boldsymbol{w}_b^H\boldsymbol{w}_b, \tag{13}$$

expression (12) can be more compactly expressed in matrix form as

$$\alpha_b=\frac{\boldsymbol{w}_b^H\boldsymbol{K}\boldsymbol{w}_b}{2\pi\boldsymbol{w}_b^H\boldsymbol{w}_b}, \tag{14}$$

where

$$\boldsymbol{K}\triangleq\int_\Theta\boldsymbol{a}(\theta)\boldsymbol{a}^H(\theta)\,d\theta \tag{15}$$

is a positive semi-definite matrix. The maximization of $\{\alpha_b\}_{b=1}^B$ is equivalent to maximizing the numerator while keeping the denominator fixed and thus corresponds to finding the B eigenvectors of the matrix $\boldsymbol{K}$ associated with the B largest eigenvectors. The DPSS beamspace matrix is then given by

$$\boldsymbol{W}_{\mathrm{DPSS}_{B,\Theta}}=[\boldsymbol{u}_1\ \ \cdots\ \ \boldsymbol{u}_B]\in\mathbb{C}^{M\times B}, \tag{16}$$

where $\boldsymbol{u}_b$, $b=1,\ldots,B$, are the B principal eigenvectors of $\boldsymbol{K}$. The appertaining DPSS beamspace snapshot vector $\tilde{\boldsymbol{x}}_{\mathrm{DPSS}}(i)$ is computed in analogy to (9). In practice, it can be assumed that prior information about the coarse location (the sector) of the sources to be estimated is available. Subsequently, the width of the sector of interest and its orientation with respect to the broadside of the array is used to select the appropriate number of beams B. In the DFT-based beamspace design, the corresponding consecutive columns of the DFT matrix have to be chosen, whereas in the DPSS-based design, B can be determined via model order selection from the eigenvalue profile of $\boldsymbol{K}$ for the spatial sector. Note that an inadequate choice of $\boldsymbol{W}$ due to an increased width and an improper spatial orientation of the sector can degrade the estimation performance of the proposed beamspace direction finding methods.

3.3. Comparison of the DFT and DPSS spatial filters

In this section, we compare the characteristics of the DFT and the DPSS spatial filters in terms of their passband transmission and their stopband attenuation. Fig. 1 shows the spatial filter response of a sensor array composed of $M=32$ elements, where the scanning angle after the beamspace transformation (7) is varied over the array

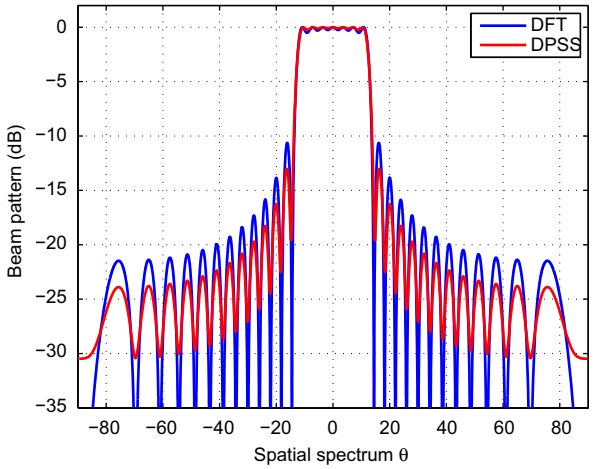

Fig. 1. Comparison of the DFT and DPSS spatial filters with $M=32$ and $B=7$.

manifold and the beam pattern $S(\theta)$ is computed by

$$S(\theta) = \|\boldsymbol{W}^H\boldsymbol{a}(\theta)\|^2 = \|\tilde{\boldsymbol{a}}(\theta)\|^2. \tag{17}$$

For the comparison in Fig. 1, $S(\theta)$ is normalized such that its maximum is equal to 1. The transformation matrix $\boldsymbol{W}$ for both filters is formed by $B=7$ beams and the sector of interest is chosen by the parameters $m=-3$ and $\Theta=[-12.5^\circ,12.5^\circ]$ for the DFT and the DPSS design, respectively. It is evident from Fig. 1 that the DFT and the DPSS filters perform similarly, but the passband of the DPSS window exhibits smaller ripples, and provides a better rejection performance in the stopband as the peaks are significantly lower. According to these observations, we expect a slightly better estimation performance of direction finding algorithms in the DPSS beamspace than in the DFT beamspace.

4. Proposed beamspace direction finding algorithms

In this section, two Krylov-based algorithms are proposed for estimating the DOAs in the beamspace.

4.1. Beamspace direction finding based on the CG algorithm

The presented BS CG algorithm is developed according to the previous work in [8] in order to reduce the dimensionality of the data and to further increase the resolution ability. The originally proposed CG method [21] is used to minimize a cost function or, equivalently, to solve a linear system of equations. It approaches the optimal solution step by step via a line search along successive directions, which are sequentially determined at each iteration. Applying the CG algorithm to beamspace direction finding [22], the system of equations, also known as the Wiener–Hopf equations, which is iteratively solved for $\tilde{\boldsymbol{w}}(\theta)$ at each scanning angle, is given by

$$\tilde{\boldsymbol{R}}\tilde{\boldsymbol{w}}(\theta) = \tilde{\boldsymbol{b}}(\theta), \tag{18}$$

where $\tilde{\boldsymbol{R}}$ is the covariance matrix of the transformed data (5) and $\tilde{\boldsymbol{b}}(\theta)$ is the initial vector depending on the search angle. However, for the CG-based DOA estimation in the beamspace, the solutions in (18) at each iteration do not have to be computed explicitly as the proposed algorithm only utilizes the orthogonal residual vectors at each step. The initialization for $\tilde{\boldsymbol{b}}(\theta)$ is defined as in [8] as

$$\tilde{\boldsymbol{b}}(\theta) = \frac{\tilde{\boldsymbol{R}}\tilde{\boldsymbol{a}}(\theta)}{\|\tilde{\boldsymbol{R}}\tilde{\boldsymbol{a}}(\theta)\|}, \tag{19}$$

where $\tilde{\boldsymbol{a}}(\theta)$, computed as in (7), is linearly transformed by the beamspace covariance matrix $\tilde{\boldsymbol{R}}$ and normalized.

The extended Krylov-based signal subspace of rank $d+1$ is generated by performing d iterations of the BS CG algorithm summarized in Table 1. The set of orthogonal residual vectors

$$\tilde{\boldsymbol{G}}_{d+1}(\theta) = \left[\tilde{\boldsymbol{b}}(\theta)\ \tilde{\boldsymbol{g}}_1(\theta)\ \cdots\ \tilde{\boldsymbol{g}}_d(\theta)\right], \tag{20}$$

where $\tilde{\boldsymbol{b}}(\theta)=\tilde{\boldsymbol{g}}_0(\theta)$ and the columns of $\tilde{\boldsymbol{G}}_{d+1}(\theta)$ span the extended Krylov subspace composed of the true signal subspace of dimension d and the scanning vector itself. All the residual vectors are normalized apart from the last one. If $\theta\in\{\theta_1,\ldots,\theta_d\}$, the initial vector $\tilde{\boldsymbol{b}}(\theta)$ lies in the true signal subspace $\boldsymbol{W}^H\boldsymbol{A}(\boldsymbol{\theta})$ and thus, the set of orthogonal residual vectors $\tilde{\boldsymbol{G}}_{d+1}(\theta)$ generated from $\tilde{\boldsymbol{b}}(\theta)$ are also contained in the column space of $\boldsymbol{W}^H\boldsymbol{A}(\boldsymbol{\theta})$, which was proven for the element space in [8]. In this case, $\tilde{\boldsymbol{G}}_{d+1}$ is not a basis for the true signal subspace in the beamspace domain so that the rank of the generated Krylov signal subspace drops from $d+1$ to d. This implies that since the last unnormalized residual vector $\tilde{\boldsymbol{g}}_d(\theta)$ cannot be a linear combination of the previously formed residual vectors due to the orthogonality to them, the following equation must hold:

$$\tilde{\boldsymbol{g}}_d(\theta) = \boldsymbol{0}. \tag{21}$$

However, if $\theta\notin\{\theta_1,\ldots,\theta_d\}$, $\tilde{\boldsymbol{G}}_{d+1}(\theta)$ is an orthogonal basis for the extended signal subspace in the beamspace domain.

In order to exploit this observation, the spectral function of the proposed BS CG direction finding algorithm is given as in [7] by

$$\tilde{P}(\theta^{(n)}) = \frac{1}{\left\|\tilde{\boldsymbol{g}}_d^H(\theta^{(n)})\tilde{\boldsymbol{G}}_{d+1}(\theta^{(n-1)})\right\|^2}, \tag{22}$$

Table 1
The proposed BS CG algorithm.

Beamspace transformation
$\tilde{\boldsymbol{x}}(i)=\boldsymbol{W}^H\boldsymbol{x}(i)$, $\tilde{\boldsymbol{a}}(\theta^{(n)})=\boldsymbol{W}^H\boldsymbol{a}(\theta^{(n)})$
for each angle $\theta^{(n)}$
  $\tilde{\boldsymbol{d}}_1(\theta^{(n)})=\tilde{\boldsymbol{g}}_0(\theta^{(n)})=\tilde{\boldsymbol{b}}(\theta^{(n)})$, $\tilde{\rho}_0(\theta^{(n)})=\tilde{\boldsymbol{g}}_0^H(\theta^{(n)})\tilde{\boldsymbol{g}}_0(\theta^{(n)})$
  for $k=1,\ \ldots,\ d$
    $\tilde{\boldsymbol{v}}_k(\theta^{(n)})=\tilde{\boldsymbol{R}}\tilde{\boldsymbol{d}}_k(\theta^{(n)})$
    $\tilde{\alpha}_k(\theta^{(n)})=[\tilde{\boldsymbol{d}}_k^H(\theta^{(n)})\tilde{\boldsymbol{v}}_k(\theta^{(n)})]^{-1}\tilde{\rho}_{k-1}(\theta^{(n)})$
    $\tilde{\boldsymbol{g}}_k(\theta^{(n)})=\tilde{\boldsymbol{g}}_{k-1}(\theta^{(n)})-\tilde{\alpha}_k(\theta^{(n)})\tilde{\boldsymbol{v}}_k(\theta^{(n)})$
    $\tilde{\rho}_k(\theta^{(n)})=\tilde{\boldsymbol{g}}_k^H(\theta^{(n)})\tilde{\boldsymbol{g}}_k(\theta^{(n)})$
    $\tilde{\beta}_k(\theta^{(n)})=[\tilde{\rho}_{k-1}(\theta^{(n)})]^{-1}\tilde{\rho}_k(\theta^{(n)})$
    $\tilde{\boldsymbol{d}}_{k+1}(\theta^{(n)})=\tilde{\boldsymbol{g}}_k(\theta^{(n)})+\tilde{\beta}_k(\theta^{(n)})\tilde{\boldsymbol{d}}_k(\theta^{(n)})$
  end
  $\tilde{\boldsymbol{G}}_{d+1}(\theta^{(n)})=[\tilde{\boldsymbol{b}}(\theta^{(n)}),\tilde{\boldsymbol{g}}_1(\theta^{(n)}),\ldots,\tilde{\boldsymbol{g}}_d(\theta^{(n)})]$
  $\tilde{P}(\theta^{(n)})=\|\tilde{\boldsymbol{g}}_d^H(\theta^{(n)})\tilde{\boldsymbol{G}}_{d+1}(\theta^{(n-1)})\|^{-2}$
end

where $\theta^{(n)}$ is defined as the current search step in the entire angular range $\{-90^\circ, \ldots, 90^\circ\}$ with $\theta^{(n)} = n \cdot \Delta^\circ - 90^\circ$, where Δ° is the search grid and $n = 0,1,\ldots,180^\circ/\Delta^\circ$. The matrix $\tilde{\boldsymbol{G}}_{d+1}(\theta^{(n-1)})$ contains all the residual vectors at the $(n-1)$th angle and $\tilde{\boldsymbol{g}}_d(\theta^{(n)})$ is the last residual vector calculated at the current search step n. If $\theta^{(n)} \in \{\theta_1, \ldots, \theta_d\}$, then $\tilde{\boldsymbol{g}}_d(\theta^{(n)}) = \boldsymbol{0}$ and we expect a peak in the pseudo spectrum.

In practical applications, the true covariance matrix in the beamspace domain $\tilde{\boldsymbol{R}}$ is unknown and needs to be estimated. Thus, the terms $\tilde{\boldsymbol{g}}_d(\theta^{(n)})$ and $\tilde{\boldsymbol{G}}_{d+1}(\theta^{(n-1)})$ in the denominator become approximations and as a result, the spectral function defined in (22) will merely provide a very large value but not approach infinity as for the true covariance matrix. Eventually, a peak search algorithm is applied to obtain the signal directions $\boldsymbol{\theta}$ from the d largest peaks of the pseudo spectrum.

4.2. Beamspace direction finding based on the AVF algorithm

In the development of the BS AVF algorithm, the concept of iteratively generating a non-eigenvector basis for the signal subspace and the search for the rank collapse of the extended Krylov signal subspace is the same as for the CG-based version. However, this approach employs the AVF algorithm to solve the system of equations in (18) iteratively for each search angle by utilizing successive auxiliary vectors. The AVF algorithm was firstly applied to sensor signal processing by the adaptive filtering work in [23] and was then exploited for direction finding in [7]. Here, the latter algorithm is extended to the operation in beamspace.

According to the previous section, we start our development with the initial vector $\tilde{\boldsymbol{b}}(\theta)$, also defined as $\tilde{\boldsymbol{b}}(\theta) = \tilde{\boldsymbol{w}}_0(\theta) = \tilde{\boldsymbol{g}}_0(\theta)$, given in (19) after performing the beamspace transformation. Then, we find d auxiliary vectors $\tilde{\boldsymbol{g}}_k(\theta)$, $k=1, \ldots, d$, that are orthogonal with respect to the previous iteration $\tilde{\boldsymbol{w}}_{k-1}(\theta)$ to solve (18), and to each other, where the first $d-1$ auxiliary vectors are also of unit norm. The auxiliary vectors are determined by maximizing the magnitude of the cross-correlation between $\tilde{\boldsymbol{w}}_{k-1}^H(\theta)\tilde{\boldsymbol{x}}(i)$ and $\tilde{\boldsymbol{g}}_k^H(\theta)\tilde{\boldsymbol{x}}(i)$. Formulating this concept as an optimization problem with respect to the orthonormality constraint for the first auxiliary vector $\tilde{\boldsymbol{g}}_1^H(\theta)$ with $\tilde{\boldsymbol{b}}(\theta) = \tilde{\boldsymbol{w}}_0(\theta)$, yields

$$\begin{aligned}\tilde{\boldsymbol{g}}_1(\theta) &= \arg\max_{\tilde{\boldsymbol{g}}_1(\theta)} \left|\mathbb{E}\{\tilde{\boldsymbol{b}}^H(\theta)\tilde{\boldsymbol{x}}(i)(\tilde{\boldsymbol{g}}_1^H(\theta)\tilde{\boldsymbol{x}}(i))^H\}\right| \\ &= \arg\max_{\tilde{\boldsymbol{g}}_1(\theta)} \left|\tilde{\boldsymbol{b}}^H(\theta)\tilde{\boldsymbol{R}}\tilde{\boldsymbol{g}}_1(\theta)\right| \\ &\quad \text{s.t. } \tilde{\boldsymbol{g}}_1^H(\theta)\tilde{\boldsymbol{b}}(\theta) = 0, \|\tilde{\boldsymbol{g}}_1(\theta)\|^2 = 1. \end{aligned} \tag{23}$$

The solution to this constrained optimization problem is obtained as

$$\tilde{\boldsymbol{g}}_1(\theta) = \frac{\left(\boldsymbol{I}_B - \tilde{\boldsymbol{b}}(\theta)\tilde{\boldsymbol{b}}^H(\theta)\right)\tilde{\boldsymbol{R}}\tilde{\boldsymbol{b}}(\theta)}{\left\|\left(\boldsymbol{I}_B - \tilde{\boldsymbol{b}}(\theta)\tilde{\boldsymbol{b}}^H(\theta)\right)\tilde{\boldsymbol{R}}\tilde{\boldsymbol{b}}(\theta)\right\|}. \tag{24}$$

The proof is given in the appendix. The recursion for the $d-1$ orthonormal auxiliary vectors with $\tilde{\boldsymbol{g}}_0(\theta) = \tilde{\boldsymbol{b}}(\theta)$ can be cast as

$$\tilde{\boldsymbol{g}}_k(\theta) = \frac{\left(\boldsymbol{I}_B - \sum_{i=0}^{k-1}\tilde{\boldsymbol{g}}_k(\theta)\tilde{\boldsymbol{g}}_k^H(\theta)\right)\tilde{\boldsymbol{R}}\tilde{\boldsymbol{w}}_{k-1}(\theta)}{\left\|\left(\boldsymbol{I}_B - \sum_{i=0}^{k-1}\tilde{\boldsymbol{g}}_k(\theta)\tilde{\boldsymbol{g}}_k^H(\theta)\right)\tilde{\boldsymbol{R}}\tilde{\boldsymbol{w}}_{k-1}(\theta)\right\|}, \tag{25}$$

and the dth auxiliary vector is the unnormalized version of (25) with $k=d$.

The iterations $\tilde{\boldsymbol{w}}_k(\theta)$ to solve the beamspace-transformed system of equations in (18) are defined as

$$\tilde{\boldsymbol{w}}_k(\theta) = \tilde{\boldsymbol{w}}_{k-1}(\theta) - \mu_k(\theta)\tilde{\boldsymbol{g}}_k(\theta), \tag{26}$$

where $\mu_k(\theta)$ is the step size, which is the solution of the minimization problem dealing with the output power described as

$$\mu_k(\theta) = \arg\min_{\mu_k(\theta)} \mathbb{E}\{\left|\tilde{\boldsymbol{w}}_{k-1}^H(\theta)\tilde{\boldsymbol{x}}(i)\right|^2\}, \tag{27}$$

and easily shown to be

$$\mu_k(\theta) = \frac{\tilde{\boldsymbol{g}}_k^H(\theta)\tilde{\boldsymbol{R}}\tilde{\boldsymbol{w}}_{k-1}(\theta)}{\tilde{\boldsymbol{g}}_k^H(\theta)\tilde{\boldsymbol{R}}\tilde{\boldsymbol{g}}_k(\theta)}. \tag{28}$$

After the computation of the d orthogonal auxiliary vectors according to the above procedure, the extended Krylov signal subspace $\tilde{\boldsymbol{G}}_{d+1}(\theta)$ in the beamspace domain, which includes the initial vector $\tilde{\boldsymbol{b}}(\theta)$ is formed, similarly to the CG-based beamspace algorithm, by

$$\tilde{\boldsymbol{G}}_{d+1}(\theta) = \left[\tilde{\boldsymbol{b}}(\theta)\ \ \tilde{\boldsymbol{g}}_1(\theta)\ \ \cdots\ \ \tilde{\boldsymbol{g}}_d(\theta)\right]. \tag{29}$$

Considering the fact that this strategy requires the computation of the vectors $\tilde{\boldsymbol{w}}_k(\theta)$ for each iteration, a direct way of obtaining the d auxiliary vectors was proposed in [24] and is summarized in Table 2 for the beamspace version.

Finally, using the previously established concept that $\tilde{\boldsymbol{g}}_d(\theta) = \boldsymbol{0}$ if $\theta \in \{\theta_1, \ldots, \theta_d\}$, we define the spectral function for the pseudo spectrum in the same fashion as in (22), yielding

$$\tilde{P}(\theta^{(n)}) = \frac{1}{\left\|\tilde{\boldsymbol{g}}_d^H(\theta^{(n)})\tilde{\boldsymbol{G}}_{d+1}(\theta^{(n-1)})\right\|^2}. \tag{30}$$

Once more $\theta^{(n)}$ is the search step in the angular range $\{-90^\circ, \ldots, 90^\circ\}$ with $\theta^{(n)} = n \cdot \Delta^\circ - 90^\circ$, where Δ° is the search grid and $n = 0,1,\ldots,180^\circ/\Delta^\circ$. Again, $\tilde{\boldsymbol{G}}_{d+1}(\theta^{(n-1)})$ contains all the auxiliary vectors at the $(n-1)$th angle,

Table 2
The proposed BS AVF algorithm.

Beamspace transformation:
$\tilde{\boldsymbol{x}}(i) = \boldsymbol{W}^H\boldsymbol{x}(i)$, $\tilde{\boldsymbol{a}}(\theta^{(n)}) = \boldsymbol{W}^H\boldsymbol{a}(\theta^{(n)})$
for each angle $\theta^{(n)}$
  $\tilde{\boldsymbol{b}}(\theta^{(n)}) = \frac{\tilde{\boldsymbol{R}}\tilde{\boldsymbol{a}}(\theta^{(n)})}{\|\tilde{\boldsymbol{R}}\tilde{\boldsymbol{a}}(\theta^{(n)})\|}$, $\tilde{\boldsymbol{g}}_1(\theta^{(n)}) = \frac{(\boldsymbol{I}_B - \tilde{\boldsymbol{b}}(\theta^{(n)})\tilde{\boldsymbol{b}}^H(\theta^{(n)}))\tilde{\boldsymbol{R}}\tilde{\boldsymbol{b}}(\theta^{(n)})}{\|(\boldsymbol{I}_B - \tilde{\boldsymbol{b}}(\theta^{(n)})\tilde{\boldsymbol{b}}^H(\theta^{(n)}))\tilde{\boldsymbol{R}}\tilde{\boldsymbol{b}}(\theta^{(n)})\|}$
  for $k = 2, \ldots, d-1$
    $\tilde{\boldsymbol{g}}_k(\theta^{(n)}) = \frac{\left(\boldsymbol{I}_B - \sum_{i=k-2}^{k-1}\tilde{\boldsymbol{g}}_i(\theta^{(n)})\tilde{\boldsymbol{g}}_i^H(\theta^{(n)})\right)\tilde{\boldsymbol{R}}\tilde{\boldsymbol{g}}_{k-1}(\theta^{(n)})}{\left\|\left(\boldsymbol{I}_B - \sum_{i=k-2}^{k-1}\tilde{\boldsymbol{g}}_i(\theta^{(n)})\tilde{\boldsymbol{g}}_i^H(\theta^{(n)})\right)\tilde{\boldsymbol{R}}\tilde{\boldsymbol{g}}_{k-1}(\theta^{(n)})\right\|}$
    $\mu_n(\theta^{(n)}) = -\mu_{n-1}(\theta^{(n)})\frac{\tilde{\boldsymbol{g}}_n^H(\theta^{(n)})\tilde{\boldsymbol{R}}\tilde{\boldsymbol{g}}_{n-1}(\theta^{(n)})}{\tilde{\boldsymbol{g}}_n^H(\theta^{(n)})\tilde{\boldsymbol{R}}\tilde{\boldsymbol{g}}_n(\theta^{(n)})}$
  end
  $\tilde{\boldsymbol{g}}_d(\theta^{(n)}) = -\mu_{d-1}(\theta^{(n)})\left(\boldsymbol{I}_B - \sum_{i=d-2}^{d-1}\tilde{\boldsymbol{g}}_i(\theta^{(n)})\tilde{\boldsymbol{g}}_i^H(\theta^{(n)})\right)\tilde{\boldsymbol{R}}\tilde{\boldsymbol{g}}_{d-1}(\theta^{(n)})$
  $\tilde{\boldsymbol{G}}_{d+1}(\theta^{(n)}) = [\tilde{\boldsymbol{b}}(\theta^{(n)}), \tilde{\boldsymbol{g}}_1(\theta^{(n)}), \ldots, \tilde{\boldsymbol{g}}_d(\theta^{(n)})]$
  $\tilde{P}(\theta^{(n)}) = \|\tilde{\boldsymbol{g}}_d^H(\theta^{(n)})\tilde{\boldsymbol{G}}_{d+1}(\theta^{(n-1)})\|^{-2}$
end

and $\tilde{\boldsymbol{g}}_d(\theta^{(n)})$ is the last unnormalized auxiliary vector calculated at the current search step n. If $\theta^{(n)} \in \{\theta_1,\ldots,\theta_d\}$, then $\tilde{\boldsymbol{g}}_d(\theta^{(n)})=\boldsymbol{0}$ and a peak occurs in the pseudo spectrum. The desired signal directions $\boldsymbol{\theta}$ are extracted from the location of the d largest peaks in the spatial spectrum.

5. Computational complexity analysis

As mentioned in the introduction, the key advantage of operating in the beamspace domain is to reduce the computational complexity linked with the conventional techniques in element space. In this section, we evaluate the computational cost of the two proposed Krylov subspace-based methods, the BS AVF and the BS CG algorithms, and compare it to the complexity of the classical direction finding methods in element space as well as their beamspace versions. We do not take into account the cost of finding $\boldsymbol{W}$ as it can be computed offline and stored for the direction finding process. Considering well-established DOA estimation algorithms, such as MUSIC [2], Root-MUSIC [3], and ESPRIT [4], the required subspace estimate is obtained using either a singular value decomposition (SVD) of the received array measurement matrix $\boldsymbol{X}$ or by computing an eigenvalue decomposition (EVD) of the estimated covariance matrix $\hat{\boldsymbol{R}}$. As the dimensions of both matrices are different, these two decompositions also cause different computational costs. Thus, we distinguish between them in the following analysis. Further insights regarding the choice between the SVD and the EVD as well as their accuracy in estimating the subspaces for practical applications can be found in [25].

5.1. Subspace estimation via the SVD

The computational cost, depicted in Table 3, is measured in terms of the number of additions and multiplications [21], where Δ° is the search step and the SVD is used for the conventional direction finding methods. The peak search in the pseudo spectrum as necessary for MUSIC, the CG algorithm, and the AVF algorithm is not considered, as there are implementations that do not require any multiplications and additions. It is evident that the BS AVF and the BS CG algorithms have a cost, which is a function of $O((180/\Delta^\circ)M^2d)$ and depends on the search grid step Δ° as the Krylov signal subspace is generated for each search angle. However, by performing the transformation into the lower dimensional beamspace, the number of sensor elements M can be replaced by B although the transformation itself has also been taken into account in Table 3.

Fig. 2 shows the complexity in terms of arithmetic operations of the analyzed algorithms as a function of the number of sensor elements M. The number of beams B is optimized for each direction finding algorithm in beamspace to provide the best estimation performance. The proposed BS CG method requires $B=5$ beams to achieve its optimal performance, whereas the proposed BS AVF, the BS MUSIC, BS Root-MUSIC, and the BS ESPRIT algorithms only demand $B=3$ beams. This is due to the iterative way of constructing the signal subspace by the

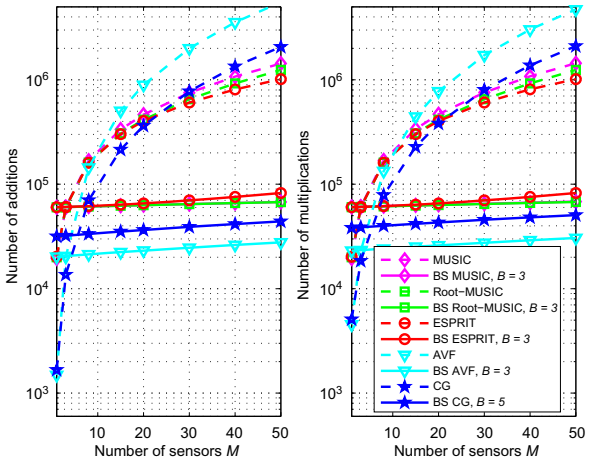

Fig. 2. Complexity in terms of arithmetic operations versus the number of sensors M applying the SVD with $d=3$, $N=50$, and $\Delta^\circ=1^\circ$.

Table 3
Computational complexity applying the SVD.

Algorithm	Multiplications	Additions
MUSIC [2]	$180/\Delta^\circ(M^2+M(2-d)-d)+8MN^2$	$180/\Delta^\circ(M^2+M(1-d)-2)+8MN^2$
BS MUSIC [10]	$180/\Delta^\circ(B^2+B(2-d)-d)+8BN^2+B(MN+M)$	$180/\Delta^\circ(B^2+B(1-d)-2)+8BN^2+B(N(M-1)+M-1)$
Root-MUSIC [3]	$2M^3-M^2d+8MN^2$	$2M^3-M^2d+M(8N^2-2)+1$
BS Root-MUSIC [17]	$B^4+3B^3+B^2(4-2d)+B(MN+8N^2-4)$	$B^4+3B^3-B^2(2d+1)+B(N(M-1)+8N^2+d)-2B+1$
ESPRIT [4]	$2M^2d+M(d^2-2d+8N^2)+8d^3-d^2$	$2M^2d+M(d^2-4d+8N^2)+8d^3-d^2+2d$
BS ESPRIT [18]	$B^2(M+3d)+B(2M^2+M(N-2)+d^2)+8BN^2+8d^3$	$B^2(M+3d-1)+B(2M^2+M(N-4)+d^2-d)+B(8N^2-N+2)+8d^3$
AVF [7]	$180/\Delta^\circ(M^2(3d+1)+M(4d-2)+d+2)+M^2N$	$180/\Delta^\circ(4dM^2+M(2d-3)-3d+2)+M^2(N-1)$
Proposed BS AVF	$180/\Delta^\circ(B^2(3d+1)+B(4d-2)+d+2)+B^2N+BM(N+1)$	$180/\Delta^\circ(4dB^2+B(2d-3)-3d+2)+B^2(N-1)+B(N(M-1)+M-1)$
CG [8]	$180/\Delta^\circ(M^2(d+1)+M(6d+2)+d+1)+M^2N$	$180/\Delta^\circ(M^2(d+1)+M(5d+1)-3d-2)+M^2(N-1)$
Proposed BS CG	$180/\Delta^\circ(B^2(d+1)+B(6d+2)+d+1)+B^2N+BM(N+1)$	$180/\Delta^\circ(B^2(d+1)+B(5d+1)-3d-2)+B^2(N-1)+B(N(M-1)+M-1)$

residual vectors in the BS CG method, which requires more input data. The curves in Fig. 2 indicate that the beamspace algorithms provide a significantly lower complexity than their counterparts in element space as M increases. Specifically, the conventional AVF- and CG-based algorithms in element space constitute a higher computational burden than the other approaches for a large array size. However, in the beamspace, the complexity of the BS AVF and the BS CG algorithms is significantly lower than that of the beamspace versions of MUSIC, Root-MUSIC, and ESPRIT, where the BS AVF algorithm requires the lowest complexity. The reason for the higher complexity of the beamspace methods for a small M is the applied transformation into the lower dimensional subspace, which increases the number of operations.

5.2. Subspace estimation via the EVD

Similarly to the previous part, in this subsection, we assess the computational complexity of the proposed BS AVF and the BS CG algorithms when the EVD is applied. As the dimensions of $\hat{\boldsymbol{R}}$ are smaller than the ones of $\boldsymbol{X}$, a lower computational burden can be expected. The required cost for the analyzed methods is shown in Table 4. Note that the expressions for the eigenvector-based methods in Table 4 also contain the necessary computation of $\hat{\boldsymbol{R}}$ from $\boldsymbol{X}$. A visual comparison is depicted in Fig. 3. The computational savings when applying the EVD translates into a lower complexity of the conventional beamspace techniques. Thus, the two proposed algorithms demand a higher computational burden. However, as their complexity depends on B, it can be further reduced by decreasing B and allowing a slight loss of the estimation performance. Also, in a practical scenario with a large dynamic range, the computation of $\hat{\boldsymbol{R}}$ may introduce finite precision errors due to the squaring of the measurement values, which deteriorate the estimation performance of the conventional BS algorithms. Furthermore, for moving sources the proposed algorithms can track the DOAs with little additional cost, whereas the SVD or EVD-based methods would require the computation of a new SVD or EVD at each snapshot.

An example showing particular values of the required additions for a specific scenario is given in Table 5.

6. Simulation results

In this section, we extensively examine the efficacy of the two proposed Krylov subspace-based algorithms in beamspace in terms of the estimation accuracy and the resolution capability and compare them to the BS MUSIC, BS Root-MUSIC, BS ESPRIT algorithms and their

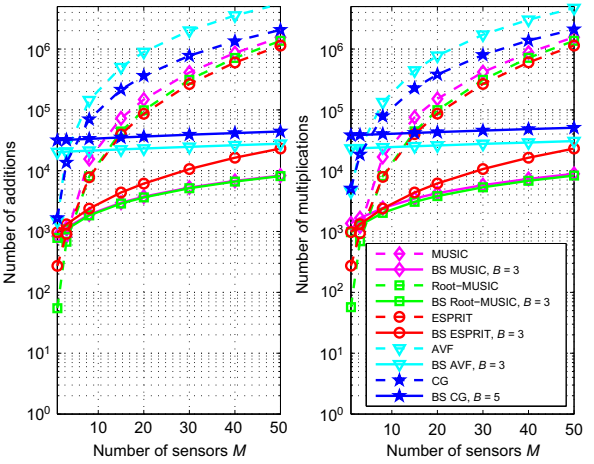

Fig. 3. Complexity in terms of arithmetic operations versus the number of sensors M applying the EVD with $d=3$, $N=50$, and $\Delta^\circ = 1^\circ$.

Table 5
Number of additions with $M=30$, $B=5$, $d=2$, $N=50$, $\Delta^\circ = 1^\circ$.

Algorithm	BS MUSIC	BS Root-MUSIC	BS ESPRIT	BS AVF	BS CG
SVD	110,635	108,176	116,609	44,800	30,580
EVD	12,860	10,401	18,834	44,800	30,580

Table 4
Computational complexity applying the EVD.

Algorithm	Multiplications	Additions
MUSIC [2]	$180/\Delta^\circ(M^2+M(2-d)-d)+8M^3+M^2N$	$180/\Delta^\circ(M^2+M(1-d)-2)+8M^3+M^2(N-1)$
BS MUSIC [10]	$180/\Delta^\circ(B^2+B(2-d)-d)+8B^3+B^2N+BM(N-1)$	$180/\Delta^\circ(B^2+B(1-d)-2)+8B^3+B^2(N-1)+B(N(M-1)+M-1)$
Root-MUSIC [3]	$10M^3+M^2(N-d)$	$10M^3+M^2(N-d-1)-2M+1$
BS Root-MUSIC [17]	$B^4+11B^3-B^2(2d-N-4)+B(MN-4)$	$B^4+11B^3-B^2(d+N)+B(N(M-1)+d-2)+1$
ESPRIT [4]	$8M^3+M^2(N+2d)+M(d^2-2d)+8d^3-d^2$	$8M^3+M^2(N+d-1)+M(d^2-4d)+8d^3-d^2+2d$
BS ESPRIT [18]	$8B^3+B^2(M+N+3d)+B(2M^2+M(N-4))+B(d^2-d-N+2)+8d^3$	$8B^3+B^2(M+N+3d-2)+B(2M^2+M(N-4))+B(d^2-d-N+2)+8d^3$
AVF [7]	$180/\Delta^\circ(M^2(3d+1)+M(4d-2)+d+2)+M^2N$	$180/\Delta^\circ(4dM^2+M(2d-3)-3d+2)+M^2(N-1)$
Proposed BS AVF	$180/\Delta^\circ(B^2(3d+1)+B(4d-2)+d+2)+B^2N+BM(N+1)$	$180/\Delta^\circ(4dB^2+B(2d-3)-3d+2)+B^2(N-1)+B(N(M-1)+M-1)$
CG [8]	$180/\Delta^\circ(M^2(d+1)+M(6d+2)+d+1)+M^2N$	$180/\Delta^\circ(M^2(d+1)+M(5d+1)-3d-2)+M^2(N-1)$
Proposed BS CG	$180/\Delta^\circ(B^2(d+1)+B(6d+2)+d+1)+B^2N+BM(N+1)$	$180/\Delta^\circ(B^2(d+1)+B(5d+1)-3d-2)+B^2(N-1)+B(N(M-1)+M-1)$

counterparts in the element space. The first part of the simulations is concerned with the comparison of the analyzed algorithms in the DFT beamspace as BS Root-MUSIC [18] and BS ESPRIT [19] are specifically developed for this beamspace design, and in the second part we compare the performance of the proposed techniques in the DFT and the DPSS beamspace.

6.1. Comparison of the proposed algorithms in the DFT beamspace

In order to evaluate the estimation performance of the proposed algorithms for closely-spaced sources in the DFT beamspace, we employ a ULA consisting of $M=10$ omnidirectional sensors with interelement spacing $\Delta=\lambda_c/2$. We assume that there are two uncorrelated complex Gaussian signals with equal power $\sigma^2=1$ impinging on the array, which are located at 35° and 40°, where the angles of arrival are measured with respect to the broadside of the array. Furthermore, we assume *a priori* knowledge about the approximate positions of the DOAs to select the sector of interest as $m=2$. The number of available snapshots at the array output is $N=50$ and each curve is obtained by averaging a total of $T=3000$ trials. In order to obtain accurate results, we set the search grid step to $\Delta^\circ=0.1^\circ$.

In the first experiment, the resolution performance of the BS AVF and the BS CG algorithms is assessed in comparison to the conventional beamspace techniques. Fig. 4 shows the probability of resolution as a function of the SNR, where the number of beams B for each direction finding algorithm in beamspace is optimized to yield the best performance. The expression for the SNR is given by

$$\mathrm{SNR}=\frac{P_s}{P_n}, \tag{31}$$

where P_s and P_n are the signal and the noise power, respectively. The signal sources are said to be resolved in a given run if both estimates $\hat{\theta}_1$ and $\hat{\theta}_2$ simultaneously fulfill the criterion [7]

$$|\hat{\theta}_l-\theta_l|<\frac{|\theta_1-\theta_2|}{2},\quad l=1,2. \tag{32}$$

It is evident from Fig. 4 that the resolution capability of the algorithms in beamspace is generally higher compared to their counterparts in element space, since *a priori* knowledge about the approximate positions of the sources is exploited. However, this is not necessarily the case for the proposed BS AVF algorithm whose resolution performance is slightly worse than its counterpart in element space for an SNR between -3 dB and 5 dB. This behavior for relatively high SNRs can be explained by the gaps between the overlapping DFT beams, which may cause parts of the signal energy to be attenuated, if the sources are unfavorably placed. In our comparison, the proposed BS CG algorithm outperforms the CG algorithm and demonstrates the best ability to resolve the two sources among the existing methods in beamspace and in element space. Here, the BS CG algorithm reaches its best performance for $B=5$ beams, while the BS AVF method and the eigenvector-based schemes attain their maximum for only $B=3$ beams.

In Fig. 5, the probability of resolution is illustrated as a function of the number of snapshots N. In order to evaluate the performance under severe conditions, the SNR is fixed at -7 dB. The BS CG algorithm clearly outperforms all the analyzed direction finding techniques in beamspace and element space, and is able to resolve the two sources at such a low SNR with more than 50 percent probability using only $N=20$ snapshots. Also, it can be seen that the BS AVF algorithm substantially improves the resolution performance of its counterpart but is outperformed by BS ESPRIT and BS Root-MUSIC. We also verify that BS MUSIC, MUSIC, Root-MUSIC, ESPRIT, and the AVF algorithm almost completely fail to separate the two sources under these severe conditions.

In the next part, the estimation accuracy is investigated in terms of the root mean square error (RMSE),

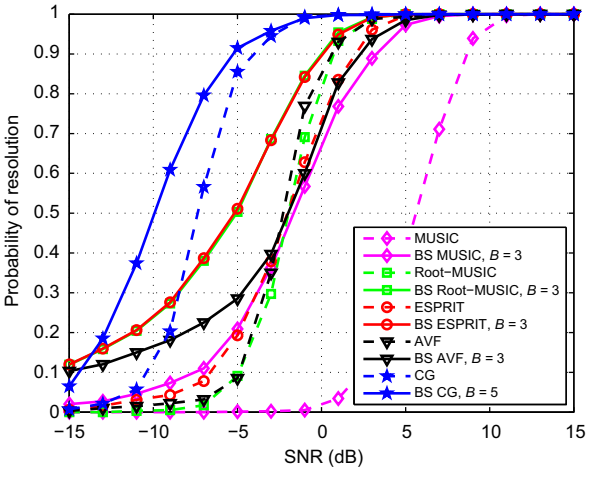

Fig. 4. Probability of resolution versus the SNR in the DFT beamspace with $M=10$, $\theta_1=35^\circ$, $\theta_2=40^\circ$, $N=50$, $m=2$.

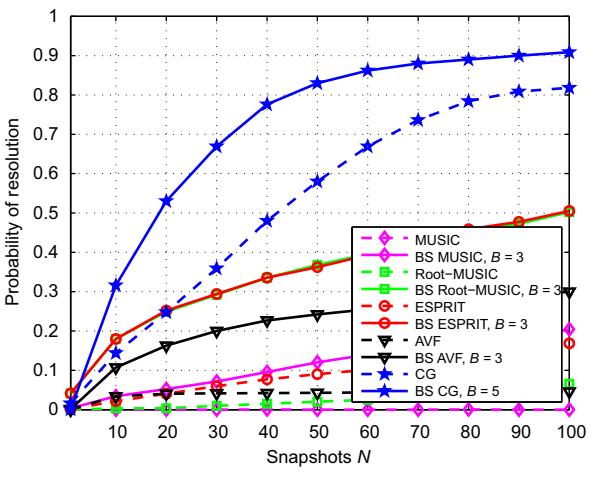

Fig. 5. Probability of resolution versus the number of snapshots N in the DFT beamspace with $M=10$, $\theta_1=35^\circ$, $\theta_2=40^\circ$, SNR$=-7$ dB, $m=2$.

where the RMSE is estimated using T trials by

$$\mathrm{RMSE}=\sqrt{\frac{1}{T}\sum_{t=1}^{T}\sum_{l=1}^{d}(\theta_l-\hat{\theta}_l(t))^2}. \tag{33}$$

The investigated direction finding algorithms in beamspace and in element space are compared to the deterministic Cramér-Rao lower bound (CRLB) [13,14]. It was established in [14] that the CRLB in beamspace is equal to the element-space CRLB if the sources are well inside the sector of interest. Since this is the case in our study, only the CRLB in the element space is depicted as a reference for the comparison. The resulting RMSE as a function of the SNR is presented in Fig. 6. Again, all the beamspace versions of the analyzed methods yield a higher estimation accuracy in the underlying scenario. However, whereas the proposed BS AVF method only provides a limited performance improvement, the BS CG algorithm outperforms the beamspace versions of ESPRIT and Root-MUSIC within the range of the SNR between -5 dB and 5 dB. Thus, applying the beamspace transformation to the original CG direction finding algorithm significantly improves the estimation accuracy for each SNR value.

Finally, in Fig. 7, we show the RMSE versus SNR performance of the proposed algorithms, where we have included the uncertainty information measured by the standard deviation around each obtained point.

6.2. Comparison of the DFT and DPSS beamspace

The aim of this section is to examine the potential of operating in the DFT and the DPSS beamspaces. It was stated in Section 3 that, apart from the applied direction finding method, the estimation performance mainly depends on the design of the beamspace transformation matrix. To this end, we compare the efficacy of the DFT and the DPSS beamspace for the two proposed Krylov subspace-based algorithms. For the simulations, the same scenario from the previous section is used to simplify the comparison and the spatial sector of interest for the DPSS beamspace is chosen as $\Theta=[25^\circ,50^\circ]$. Similarly to the DFT beamspace, the number of beams for the DPSS beamspace is optimized to yield the best results.

According to Fig. 8, the resolution performance of the DPSS BS CG algorithm versus the SNR is slightly better than that in the DFT beamspace. Furthermore, the DPSS BS AVF algorithm compensates the deficiency of the DFT version for relatively high SNRs due to its smoother passband transmission and thus provides an enhanced resolution capability for closely spaced sources.

Similar results are shown in Fig. 9, where the DPSS spatial filter yields a small improvement of the probability of resolution for both proposed beamspace techniques as the data record increases.

Fig. 10 evaluates the RMSE performance against the SNR and once more, the advantage of the DPSS beamspace becomes obvious. The proposed algorithms benefit from the transformation into the lower-dimensional DPSS

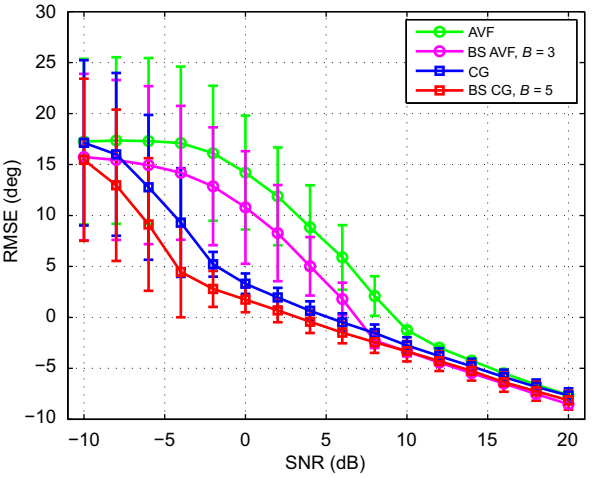

Fig. 7. RMSE versus the SNR with the standard deviation in the DFT beamspace for $M=10$, $\theta_1=35^\circ$, $\theta_2=40^\circ$, $N=50$, $m=2$.

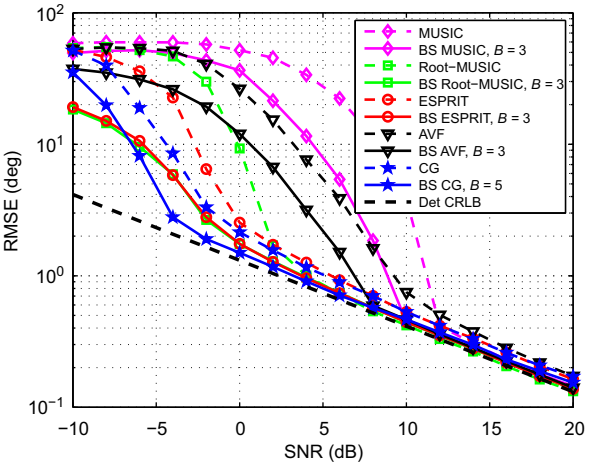

Fig. 6. RMSE versus the SNR in the DFT beamspace with $M=10$, $\theta_1=35^\circ$, $\theta_2=40^\circ$, $N=50$, $m=2$.

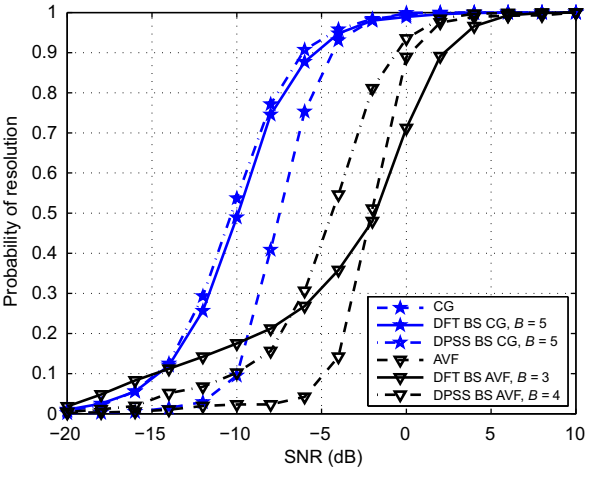

Fig. 8. Comparison of the DFT and DPSS beamspace regarding the probability of resolution versus the SNR with $M=10$, $\theta_1=35^\circ$, $\theta_2=40^\circ$, $N=50$, $m=2$.

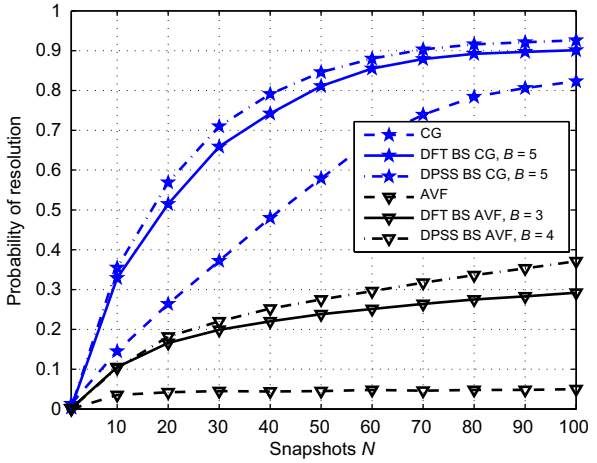

Fig. 9. Comparison of the DFT and DPSS beamspace regarding the probability of resolution versus the number of snapshots N with $M=10$, $\theta_1=35^\circ$, $\theta_2=40^\circ$, SNR$=-7$ dB, $m=2$.

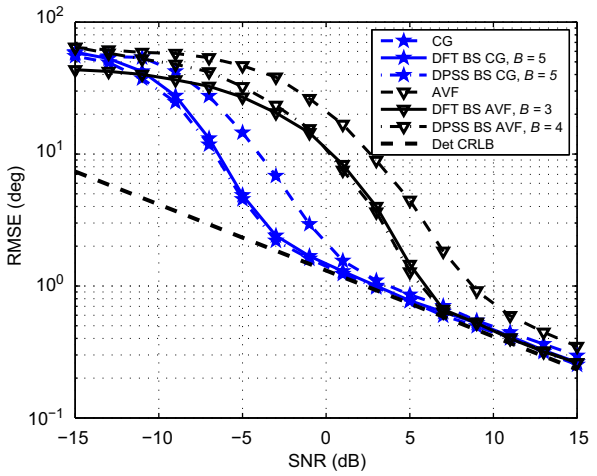

Fig. 10. Comparison of the DFT and DPSS beamspace regarding the RMSE versus the SNR with $M=10$, $\theta_1=35^\circ$, $\theta_2=40^\circ$, $N=50$, $m=2$.

beamspace, outperforming the versions associated with the DFT beamspace.

As evident from the simulation results, the spatial filter designed using DPSS tapers implies a slight performance advantage over the DFT beamspace. This behavior was already anticipated from Fig. 1 in Section 3.3 based on the fact that the DPSS filter provides a better rejection performance in the stopband.

7. Conclusion

In this paper, two Krylov subspace-based techniques are developed for direction finding in the beamspace domain as an extension of the recently proposed AVF algorithm and the CG algorithm for DOA estimation in the element space. The presented beamspace methods significantly improve the estimation accuracy of their counterparts for closely spaced sources at low SNRs using a small data record size. As both algorithms iteratively generate the signal subspace in the beamspace domain, they do not resort to an eigendecomposition of the signal covariance matrix. To verify the beamspace-related reduction of the computational burden, an extensive analysis of the complexity requirements is conducted. Also, it is shown that operation in beamspace substantially enhances the resolution capability and the estimation accuracy, where the BS CG outperforms the BS AVF algorithm, which may have a worse RMSE performance than the classical beamspace methods for widely-spread sources in the beamspace sector. In addition, two different ways of designing the beamspace, namely the discrete Fourier transform (DFT) and the discrete prolate spheroidal sequences (DPSS) beamspace are analyzed and compared. It is demonstrated that the proposed algorithms in the DPSS beamspace provide a higher estimation performance than in the DFT beamspace.

Appendix

Noticing that the cost function and the constraints are phase invariant, we can, without loss of generality, restrict $\tilde{\boldsymbol{b}}^H(\theta)\tilde{\boldsymbol{R}}\tilde{\boldsymbol{g}}_1(\theta)$ to be real-valued and non-negative, i.e., $\tilde{\boldsymbol{b}}^H(\theta)\tilde{\boldsymbol{R}}\tilde{\boldsymbol{g}}_1(\theta)\geq 0$. Thus, the Lagrange function is formed as

$$L(\tilde{\boldsymbol{g}}_1(\theta))=\tilde{\boldsymbol{g}}_1^H(\theta)\tilde{\boldsymbol{R}}\tilde{\boldsymbol{b}}(\theta)-\lambda_1\tilde{\boldsymbol{g}}_1^H(\theta)\tilde{\boldsymbol{b}}(\theta)-\lambda_2(\tilde{\boldsymbol{g}}_1^H(\theta)\tilde{\boldsymbol{g}}_1(\theta)-1). \tag{34}$$

Taking the gradient with respect to $\boldsymbol{g}_1^*(\theta)$ and equating it to zero, we obtain

$$\tilde{\boldsymbol{g}}_1(\theta)=\lambda_2^{-1}(\tilde{\boldsymbol{R}}\tilde{\boldsymbol{b}}(\theta)-\lambda_1\tilde{\boldsymbol{b}}(\theta)). \tag{35}$$

The enforcement of the constraints in (23) leads to a system of equations that is solved for λ_1 and λ_2 by

$$\lambda_1=\frac{\tilde{\boldsymbol{b}}^H(\theta)\tilde{\boldsymbol{R}}\tilde{\boldsymbol{b}}(\theta)}{\|\tilde{\boldsymbol{b}}(\theta)\|^2}, \tag{36}$$

and

$$\lambda_2=\left\|\tilde{\boldsymbol{R}}\tilde{\boldsymbol{b}}(\theta)-\frac{\tilde{\boldsymbol{b}}^H(\theta)\tilde{\boldsymbol{R}}\tilde{\boldsymbol{b}}(\theta)}{\|\tilde{\boldsymbol{b}}(\theta)\|^2}\tilde{\boldsymbol{b}}(\theta)\right\|. \tag{37}$$

After inserting (36) and (37) into (35), considering the fact that $\|\tilde{\boldsymbol{b}}(\theta)\|^2=1$, and some straightforward operations, we arrive at the desired result

$$\tilde{\boldsymbol{g}}_1(\theta)=\frac{\left(\boldsymbol{I}_B-\tilde{\boldsymbol{b}}(\theta)\tilde{\boldsymbol{b}}^H(\theta)\right)\tilde{\boldsymbol{R}}\tilde{\boldsymbol{b}}(\theta)}{\left\|\left(\boldsymbol{I}_B-\tilde{\boldsymbol{b}}(\theta)\tilde{\boldsymbol{b}}^H(\theta)\right)\tilde{\boldsymbol{R}}\tilde{\boldsymbol{b}}(\theta)\right\|} \tag{38}$$

for the maximization of the cross-correlation subject to the imposed constraints, which completes the proof.

References

[1] H. Krim, M. Viberg, Two decades of array signal processing research: parametric approach, IEEE Signal Processing Magazine 13 (4) (1996) 67–94.
[2] R.O. Schmidt, Multiple emitter location and signal parameter estimation, IEEE Transactions on Antennas and Propagation 34 (3) (1986) 276–280.

[3] A. Barabell, Improving the resolution performance of eigenstructure-based direction-finding algorithms, in: IEEE International Conference on Acoustics, Speech, and Signal Processing, 1983, pp. 336–339.
[4] R.H. Roy, T. Kailath, ESPRIT—estimation of signal parameters via rotational invariance techniques, IEEE Transactions on Acoustics, Speech, and Signal Processing 37 (7) (1989) 984–995.
[5] M.L. Honig, J.S. Goldstein, Adaptive reduced-rank interference suppression based on the multistage Wiener filter, IEEE Transactions on Communications 50 (6) (2002) 986–994.
[6] R.C. de Lamare, M. Haardt, R. Sampaio-Neto, Blind adaptive constrained reduced-rank parameter estimation based on constant modulus design for CDMA interference suppression, IEEE Transactions on Signal Processing 56 (6) (2008) 2470–2482.
[7] R. Grover, D.A. Pados, M.J. Medley, Subspace direction finding with an auxiliary-vector basis, IEEE Transactions on Signal Processing 55 (2) (2007) 758–763.
[8] H. Semira, H. Belkacemi, S. Marcos, High-resolution source localization algorithm based on the conjugate gradient, EURASIP Journal on Advances in Signal Processing 2007 (2) (2007) 1–9.
[9] C.E. Chen, F. Lorenzelli, R.E. Hudson, K. Yao, Stochastic maximum-likelihood DOA estimation in the presence of unknown nonuniform noise, IEEE Transactions on Signal Processing 56 (7) (2008) 3038–3044.
[10] A. Seghouane, A Kullback–Leibler methodology for unconditional ML DOA estimation in unknown nonuniform noise, IEEE Transactions on Aerospace and Electronic Systems 47 (4) (2011) 3012–3021.
[11] G. Bienvenu, L. Kopp, Decreasing high resolution method sensitivity by conventional beamformer preprocessing, in: IEEE International Conference on Acoustics, Speech, and Signal Processing, 1984, pp. 714–717.
[12] H. Lee, M. Wengrovitz, Resolution threshold of beamspace MUSIC for two closely spaced emitters, IEEE Transactions on Acoustics, Speech, and Signal Processing 38 (9) (1990) 1545–1559.
[13] S. Anderson, On optimal dimension reduction for sensor array signal processing, Elsevier Signal Processing 30 (1993) 245–256.
[14] H.V. Trees, Optimum Array Processing: Part IV of Detection, Estimation, and Modulation Theory, John Wiley & Sons, 2002.
[15] A. Hassanien, S.A. Elkader, A.B. Gershman, K.M. Wong, Convex optimization based beam-space preprocessing with improved robustness against out-of-sector sources, IEEE Transactions on Signal Processing 54 (5) (2006) 1587–1595.
[16] A. Hassanien, S. Vorobyov, A robust adaptive dimension reduction technique with application to array processing, IEEE Signal Processing Letters 16 (1) (2009) 22–25.
[17] M. Rübsamen, A.B. Gershman, Direction-of-arrival estimation for nonuniform sensor arrays: from manifold separation to Fourier domain MUSIC methods, IEEE Transactions on Signal Processing 57 (2) (2009) 588–599.
[18] M.D. Zoltowski, G.M. Kautz, S.D. Silverstein, Beamspace root-MUSIC, IEEE Transactions on Signal Processing 41 (1) (1993) 344–364.
[19] G. Xu, S.D. Silverstein, R.H. Roy, T. Kailath, Beamspace ESPRIT, IEEE Transactions on Signal Processing 42 (2) (1994) 349–356.
[20] P. Forster, G. Vezzosi, Application of spheroidal sequences to array processing, in: IEEE International Conference on Acoustics, Speech, and Signal Processing, Dallas, USA, 1987, pp. 2268–2271.
[21] G.H. Golub, C.F. Loan, Matrix Computations, 3rd ed. Johns Hopkins University Press, Baltimore, MD, 1996.
[22] J. Steinwandt, R.C. de Lamare, M. Haardt, Beamspace direction finding based on the conjugate gradient algorithm, in: IEEE International ITG Workshop on Smart Antennas, Aachen, Germany, 2011.
[23] D.A. Pados, G.N. Karystinos, An iterative algorithm for the computation of the MVDR filter, IEEE Transactions on Signal Processing 49 (2) (2001) 290–300.
[24] W. Chen, U. Mitra, P. Schniter, On the equivalence of three reduced rank linear estimators with applications to DS-CDMA, IEEE Transactions on Information Theory 48 (9) (2002) 2609–2614.
[25] E.S. Baker, R.D. DeGroat, Evaluating EVD and SVD errors in signal processing environments, in: Conference Record of the Thirty-Second Asilomar Conference on Signals, Systems and Computers, vol. 2, 1998, pp. 1027–1032.